# Pellet Triggering Type-I Edge Localized Modes in Tokamaks


## Abstract

The phenomena of Type-I Edge Localized Modes (ELMs), also known as "Giant" ELMs, within tokamak plasmas and their triggering via pellet injection are detailed. Ideal ballooning modes and their coupling with external "peeling" modes provide a description for Type-I ELM origination, so their physics are also described. Type-I ELMs transport heat and particles to plasma facing components (PFCs), degrading tokamak longevity, so researchers seek mitigation. One such mitigation technique, pellet triggering, includes a rich technological history to which Futatani and Hu, among many others, have recently generated nonlinear, extended MHD models for further understanding. The progress of pellet-triggering ELMs and an experimental comparison of these models is thus provided. Finally, a discussion on pellet-pacing's future, potential resolutions to its short-comings, and open issues is provided.


## Introduction

Technological progress in tokamaks increased magnetic confinement into new operational spaces with distinct characteristics, such as the high-confinement H-Mode. Interestingly, H-Mode plasmas demonstrate a steep pressure gradient concentrated at the plasma edge, which unlocks previously unseen phenomena like the edge-transport barrier (ETB) and edge-localized modes (ELMs). "Edge", or Scrap-Off Layer (SOL) in divertor plasmas, denotes a region of open flux surfaces beyond the magnetic separatrix, and extending to the plasma's exterior, which ends a small distance before the tokamak's first wall. Figure 1 simply depicts this configuration [1].

In H-Modes, researchers observe periodic instabilities "burping" the peripheral plasma along open field lines onto plasma-facing components (PFCs) like the divertor targets and leaving behind residual magnetohydrodynamic (MHD) signatures. This is essentially a reduction of the edge pressure gradient and global confinement as shown in Figure 2 [2]. These Type-I "Giant" ELMs damage PFCs by excessive heat fluxes and sputtering thereby compromising longevity of expensive experimental reactors. Other ELM types exist but are beyond the scope of this paper.

Although ELM-free, H-Mode discharges have been achieved, stationary function requires some ELM activity [3]. Type-I ELMs, hereafter referred to as ELMs, exhaust impurities and control plasma density profiles like a natural blowoff valve. Striking a balance between ELM amplitude and frequency for steady-state H-Mode operation is an ongoing challenge for researchers. Techniques for ELM mitigation include gas puffing, magnetic field perturbations, and pellet pacing, the latter which is emphasized in later sections.

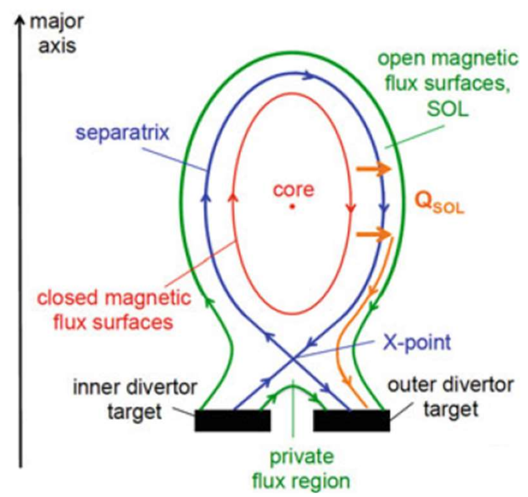


*Figure 1 – Poloidal cross-section schematic in tokamak with poloidal divertors [1].*

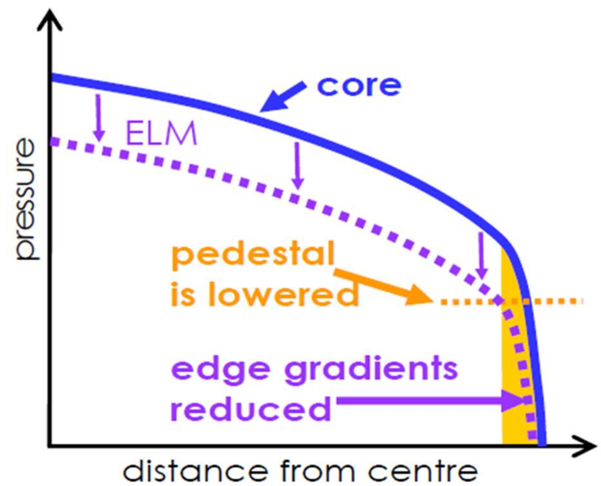


*Figure 2 - H-Mode plasma pressure plotted relative to minor radius with effect of ELM event [2].*

# Type-I Edge Localized Modes

Managing ELMs requires an understanding of them. An introduction to their evolution and characteristics is thus given with depth into the theorized cause – coupled peeling-ballooning modes.

## Experimental Observation

Figure 3 depicts an ELM's evolution relative to measured alpha particle flux and magnetic field perturbations [4]. The ELM occurs in the range of 100 μs without clear magnetic precursor signal, and all consequences decay within about a millisecond! Typically, 5-15% of stored plasma energy may be expelled during such an event. Increased plasma temperature increases the expulsion by reducing particle collisionality, but the range scales well with machine size. ELM severity and frequency is more noticeable in Figure 4 by comparison to Type-III ELMs [5]. Although ELM frequency shows some consistency in Figure 4, it can vary greatly between machines and operating parameters. ITER's natural ELM frequency may be sub-1 Hz, while other machines reach 200 Hz [5,3]. Most noticeable in ELM dynamics is the effect of plasma shaping, specifically triangularity. Finally, the Figure 4 temperature ($T_e$) and density ($n_{e,edge}$) plots demonstrate "saturations" that occur far beyond Type-III ELM conditions.

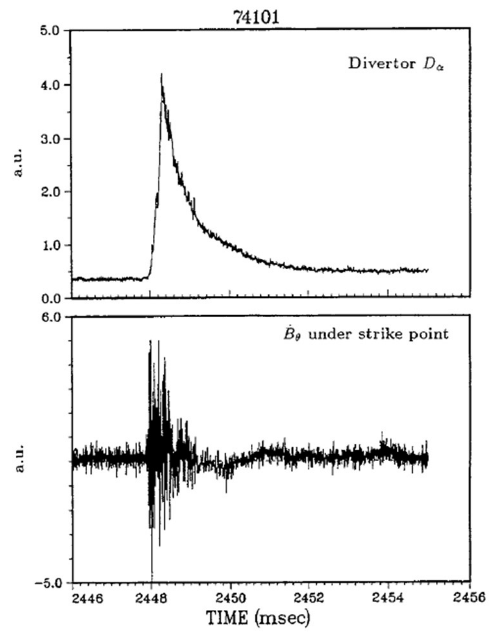


*Figure 3 – (Left) Divertor alpha particle flux and magnetic field perturbation rate from DIII-D discharge with Type-I ELM [4].*

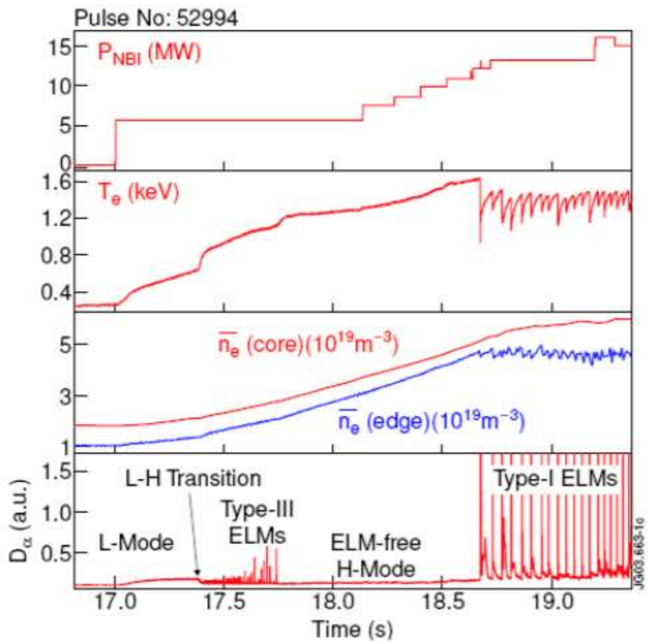


*Figure 4 - Measurements of extended discharge time demonstrating variability of ELMs (Type-I and others) [5].*

A common observation at an ELM's onset regardless of machine is dependence on local pressure gradient, α (equation 1), like predicted by ideal ballooning theory and evident in Figure 4's $n_{e,edge}$ fluctuations. Achieving a critical pressure gradient, $\alpha_{crit}$, has been deemed a necessary but insufficient criterion for ELM triggering because of variable time lags until the ELM occurs [3]. Density fluctuations concentrated to a tokamak's LFS further indicate ballooning mode existence [6]. Including edge current helps explain hovering around $\alpha_{crit}$. Ideal external kink, or "peeling", modes rely on an edge current density, **j**, threshold hence the theorized peeling-ballooning mode coupling. Altogether, the ELM cycle may be understood per Connor, Hastie, and Wilson's 1997 theory suggesting an "edge" ballooning instability occurs before an increasing current density stabilizes it at which point a peeling instability takes over [7]. Once pressure drops enough, the ELM ceases and the plasma returns to stability where it rebuilds the parameter gradients. Figure 5 depicts the described sequence [7].

$$\alpha = -\frac{2Rq^2}{B^2}\frac{dp}{dr} \tag{1}$$

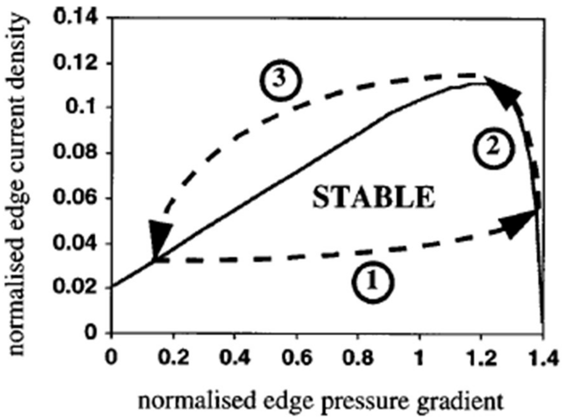


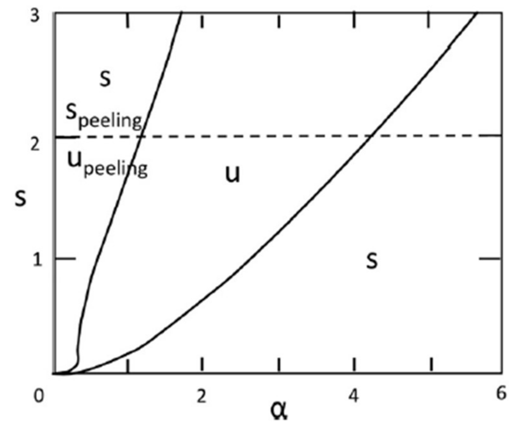


*Figure 5 – (Left) Connor, Hastie, and Wilson Peeling-Ballooning ELM Cycle [7]. (Right) Marginally stable (s) and unstable (u) regions for high-aspect ratio tokamak with respect to ballooning and peeling ($s_{peeling}$, $u_{peeling}$) for various localized, mean pressure gradient, α, and shear, S [8].*

## Coupled Peeling-Ballooning Mode

Ideal ballooning modes, with their poloidally wavy pressure fluctuations about rational flux surfaces, possess a moderate-to-high toroidal mode number. The ballooning traverses helically around the torus with two distinct length scales: a short, perpendicular wavelength (geodesic or normal) and a long, parallel wavelength. Though dependent on "bad curvature" like interchange modes, ballooning modes also rely on pressure to exceed magnetic curvature's stabilization. The ballooning mode's growth depends on plasma shear, generally "q" but locally "s" and described by equation 2, and the local pressure gradient, α, as evident in the s-α diagram of figure 5 [7,8]. While useful, conventional ballooning theory loses some validity in edge regions due to discontinuities of pressure and current density. This led to a modified, edge ballooning theory by [7].

$$s = \frac{d(lnq)}{d(lnr)} \qquad (2)$$

External, ideal peeling modes, also of high toroidal mode number, are driven by current density. Unlike the ballooning mode, resonant surfaces are beyond the plasma boundary hence "external". Stabilization may occur by pressure gradient, so interaction between peeling and ballooning – stabilized by edge current – modes naturally occurs near parameter thresholds. These instabilities can be described using the energy principle, which includes two terms directly relating to ballooning and peeling instabilities. Although beyond the scope, worth noting is that an expansion of MHD equations into a modified Fourier domain while accounting for double periodicity shows peeling harmonic coupling leading to ballooning [7].

# Pellet-Induced ELMs

## History

Cryogenically cooled pellets injected into plasmas at high velocities hold many uses. Applying the technology towards ELM production gained prevalence in the 1990s and has since been studied greatly. The concept for disruption control was simple once pellet-triggered ELMs became known: inject a sufficient pellet into plasma more frequently than natural ELMs occur and the ELM's heat flux tends to be lower than its natural range. Lang suggested conservation of the ELM frequency and energy loss per ELM product, further justifying pellet pacing [9]. While "pellet pacing" is simple, the technique's details are critical. Pellet variables include geometry, material, velocity, frequency, and location among other things. Improper parameters can fail to trigger an ELM; asymmetrically load divertors; damage PFCs with unablated fragments; and generate a disruption by over-fueling or under-exhausting. Pellet shattering, simultaneous injection, on-demand pellet variation, and hollow pellets are all relatively recent innovations aimed at minimizing these downfalls.

## Phenomenology

As a frozen pellet crosses the plasma separatrix its outer surface sublimates into a neutral gas shield. Portions of the neutral gas ionize and expand, while the freshly exposed pellet exterior also sublimates, and the process continuously repeats. Released electrons spread in the form of a thermal-speed cooling wave, while ions travel at the ion sound speed. This occurs while the pellet traverses the plasma chamber at 25-1000 m/sec on a nearly straight trajectory due to neutral gas shielding (NGS). The ablation rate partially determines a pellet's subsequent density perturbation, which must be sufficient for ELM triggering. Parks' 1978 model for an adiabatic, velocity-dependent ablation rate is widely accepted for such a case. Integration of equation 2 along the pellet trajectory, l, provides an ablation rate, $N_p$ [10]. Here, $r_p$ is the spherical pellet radius, $n_e$ is the electron density, and $T_e$ is the electron temperature.

$$V_p \frac{dN_p}{dl} = -(Constant) r_p^{4/3} n_e^{1/3} T_e^{1.64} \tag{1}$$

For a spherical pellet, the constant of (1) is experimentally determined at a particular velocity and the ablation rate is approximately as given in equation 2 [11]. (1) and (2) should obtain different form for different pellet shapes.

$$N_p = 4.12 \times 10^{16} r_p^{4/3} n_e^{1/3} T_e^{1.64} \tag{2}$$

Kocsis, et al. proposed a minimum penetrating distance, $L_{seed}$, defined by the distance between separatrix and a critical flux surface, where the pellet's density perturbation – <10% of the pellet mass – can spread [12]. $L_{seed}$ was determined with a high accuracy to be midway into the plasma edge pedestal, which aligns with the peak pressure gradient. Helical magnetic field lines transport the newly charged particles from their source, forming a locally elevated pressure band as shown in Figure 6 [11]. As the perturbation spreads its temperature rapidly increases thereby pushing past the previously mentioned $\alpha_{crit}$ and triggering the ELM like usual.

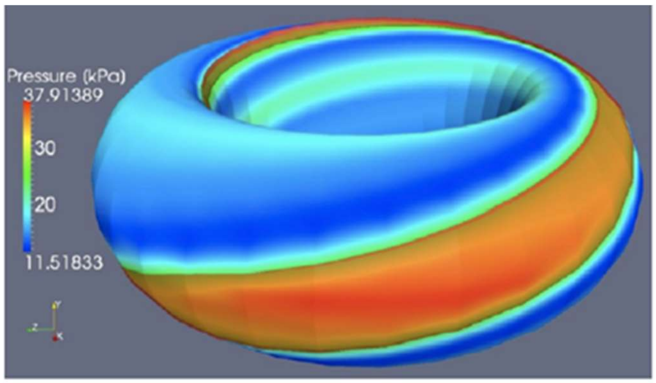


*Figure 6 - Plasma pressure after pellet injection calculated by JOREK code where red and orange indicate the pellet's transported perturbation [11]*

## Nonlinear, Reduced MHD Modeling

The transient, three-dimensional dynamics of ELMs and pellet pacing them provides limited use for linear analysis, so nonlinear, reduced resistive-MHD codes are generally deployed. JOREK is one such package applied towards pellet-induced ELM research in tokamaks. JOREK's governing equations in toroidal coordinates (R = major radius, Z = vertical coordinate, φ = toroidal angle) with descriptions in parentheses and parameter definitions are given by equations 3a-3j and table 1, respectively [13]. These equations are resolved in finite element fashion with implicit time stepping.

$$\vec{B} = F_0 \nabla\phi + \nabla\psi \times \nabla\phi \text{ (magnetic field)} \tag{3a}$$

$$\vec{v} = v_{\parallel}\vec{B} - R^2\nabla u \times \nabla\phi \text{ (velocity field)} \tag{3b}$$

$$\frac{\partial \phi}{\partial t} = \eta(T_e) R^2 \nabla \cdot (R^{-2}\nabla\psi) - Ru, \psi - F_0 \frac{\partial u}{\partial \psi} \tag{3c}$$

$$j = R^2 \nabla \cdot (R^{-2}\nabla\psi)\, , j_\phi = -j/R \text{ (Ampere's Law with Permeability)} \tag{3d}$$

$$R\nabla \cdot \left(R^2 \rho \nabla_{pol} \frac{\partial u}{\partial t}\right) = \frac{1}{2}\{R^2 \left|\nabla_{pol} u, R^2\rho\right\} + leftR^4\rho\omega, u + \{\psi, j\} - \frac{F_0}{R}\frac{\partial j}{\partial \phi} + \{\rho T, R^2\} + R\mu(T_e)\nabla^2\omega - \nabla \cdot \left[\left(\rho\rho_n S_{ion}(T_e) - \rho^2 \alpha_{rec}(T_e)\right) R^2 \nabla_{pol} u\right] \text{ (Vorticity Induction)} \tag{3e}$$

$$\omega = \frac{1}{R}\frac{\partial}{\partial R}\left(R\frac{\partial u}{\partial R}\right) + \frac{\partial^2 u}{\partial Z^2} \text{ (Toroidal vorticity)} \tag{3f}$$

$$\frac{\partial \rho}{\partial t} = -\nabla \cdot (\rho\vec{v}) + \nabla \cdot (D_\perp \nabla_\perp \rho + D_\parallel \nabla_\parallel \rho) + \rho\rho_n S_{ion}(T_e) - \rho^2 \alpha_{rec}(T_e) \text{ (Continuity)} \tag{3g}$$

$$\frac{\partial(\rho T)}{\partial t} = -\vec{v} \cdot \nabla(\rho \mathrm{T}) + \gamma\rho T \nabla \cdot \vec{v} + \nabla \cdot (\backslash chi_\perp \nabla_\perp T + \backslash chi_\parallel \nabla_\parallel T) + \frac{2}{3R^2}\eta(T_e) j^2 - \xi_{ion}\rho\rho_n S_{ion}(T_e) - \rho\rho_n P_L(T_e) - \rho^2 P_B(T_e) \text{ (Pressure)} \tag{3h}$$

$$\rho B^2 \frac{\partial v_\parallel}{\partial t} = -\rho \frac{F_0}{2R^2}\frac{\partial}{\partial \phi}\left(B^2 v_\parallel^2\right) - \frac{\rho}{2R}\left\{B^2 v_\parallel^2, \psi\right\} - \frac{F_0}{R^2}\frac{\partial(\rho T)}{\partial \phi} + \frac{1}{R}\psi, \rho T + B^2 \mu_\parallel(T_e) \nabla_{pol}^2 v_\parallel + \left(\rho^2 \alpha_{rec}(T_e) - \rho\rho_n S_{ion}(T_e)\right) B^2 v_\parallel \text{ (Parallel Momentum)} \tag{3i}$$

$$\frac{\partial \rho_n}{\partial t} = \nabla \cdot \left(\overrightarrow{D_n} \cdot \nabla \rho_n\right) + \rho^2 \alpha_{rec}(T_e) - \rho\rho_n S_{ion}(T_e) + S_n \text{ (Diffusive Neutral Species Density)} \tag{3j}$$

| Parameter | Symbol | Parameter | Symbol |
|---|---|---|---|
| $T_s$ | Species Temperature | ρ | Density |
| μ | Viscosity | ξ | Ionization Energy |
| η | Resistivity | S | Ionization Rate |
| κ | Thermal Conductivity | P | Radiation Power |
| α | Recombination Rate | D | Diffusion Coefficient |

*Table 1 - Key JOREK Parameters*

Pairing JOREK with ablation equations (1)-(2) to represent neutral gas shielding, Futatani simulated various pellet injection scenarios into the DIII-D tokamak. For validation before pellet injection, toroidal mode number n=10 energy was analyzed relative to critical pedestal pressure with DIII-D operating parameters. Results matched expectations regarding stability limits and are given in figure 7 [11].

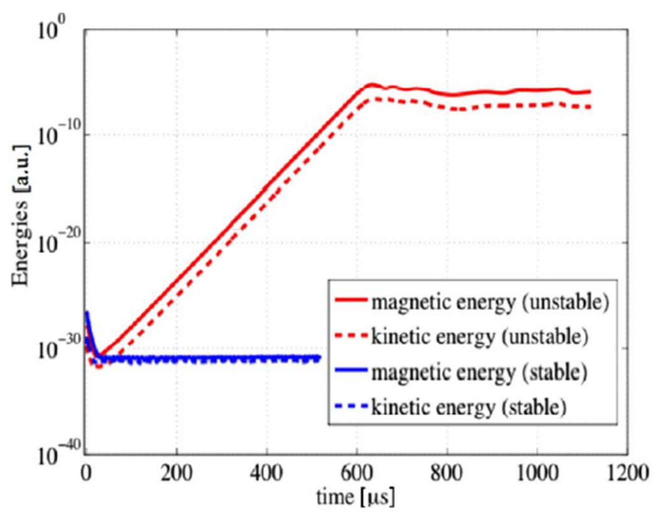


*Figure 7 - JOREK-produced toroidal mode number n=10 energy vs time with sub-critical (stable) and critical (unstable) pedestal pressure [11]*

Futatani later demonstrated variability in ELM triggering related to pellet size, velocity, location, and trajectory, like Lang and others have shown experimentally. An important result was divertor heat flux asymmetries, which appear 180 degrees toroidally from injection point and on the outer divertor. Figure 8 depicts this adequately [11]. Finally, modeling with and without the SOL showed little effect on MHD activity and pellet requirements.

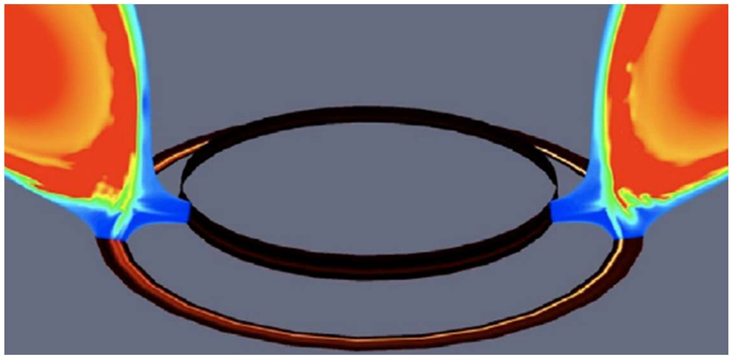

*Figure 8 - Asymmetry of divertor heat flux resulting from pellet-induced ELM [11].*

Despite the promising outputs from codes like JOREK, compromises are generally necessary. One such issue is the spatiotemporal scale difference between the pellet cloud’s evolution and global MHD activity. Futatani notes an artificially larger cloud due to mesh granularity at the smaller scales, and this likely relates to an overestimate of pellet size required for ELM triggering. Additionally, inner-to-outer divertor heat flux asymmetry in DIII-D falls short of simulations, and this error’s origin remains unknown. Finally, although turbulence is greatly reduced in H-mode SOLs, any provocation of turbulence by pellet injection lacks consideration with MHD approaches.

# Discussion

Introductory tokamak edge physics have been elucidated along with Type-I ELMs. Experimental observation of ELMs and the prevailing theory of their cycling in H-Modes via peeling-ballooning modes was presented to appreciate pellet-pacing’s mechanism. Descriptions of pellet-pacing physics were outlined along with modeling via nonlinear, reduced MHD modeling. Benefits and downfalls to each of these have also been mentioned.

All said, is pellet pacing the appropriate tool? Each triggered ELM, despite reduced severity relative to natural ELMs, still represents a decay in confinement with a degree of randomness. Shattered pellet and synchronized injection mitigate some of this mitigation techniques problems but lack rapid adaptability for controlling a plasma which spans many orders of magnitude in nearly every parameter. A further improvement may be on-demand injection angle variation whereby pellets can enter the plasma co- or counter-rotation toroidally and poloidally. From a modeling perspective, adaptive meshing based on empirical logic criteria or data-augmented machine learning could resolve resolution issues before adequate pellet cloud dispersion.

# References

[1] Krasheninnikov S, Smolyakov A, and Kukushkin A 2020 *On the Edge of Magnetic Fusion Devices* 3

[2] Connor J, Kirk A, and Wilson H R 2008 *AIP conference proceedings* **1013.1** 2

[3] Zohm H 1996 *Plasma physics and controlled fusion* **38.2** 105

[4] Zohm H *et al* 1995 *Nucl. Fusion* **35** 543

[5] Bhatnagar V P *et al* 1999 *Nucl. Fusion* **39** 353

[6] Kirk A *et al* 2003 *Plasma Phys. Control. Fusion* **46** 551

[7] Connor J W, Hastie R J, Wilson H R 1998 *Physics of Plasmas* **5** 2687

[8] Zheng L 2015 *Advanced Tokamak Stability* 23-36

[9] Lang P T *et al* 2003 *Nucl. Fusion* **43** 1110

[10] Parks P B, Turnbull R J 1978 *Physics of Fluids* **21** 1735

[11] Futatani S *et al* 2014 *Nucl. Fusion* **54** 073008

[12] Kocsis G *et al* 2007 *Nucl. Fusion* **47** 1166

[13] Hu D *et al* 2018 *Nucl. Fusion* **58** 126025